ACCOUNTS of chemical research

pubs.acs.org/accounts

Article

Evaporation-Induced Self-Assembly of Metal Oxide Inverse Opals: From Synthesis to Applications

Published as part of the Accounts of Chemical Research special issue "Self-Assembled Nanomaterials".

Jessi E.S. van der Hoeven,[‖] Anna V. Shneidman,[‖] Natalie J. Nicolas,[‖] and Joanna Aizenberg*

Cite This: *Acc. Chem. Res.* 2022, 55, 1809−1820

Read Online

ACCESS | Metrics & More | Article Recommendations

CONSPECTUS: Inverse opals (IOs) are highly interconnected three-dimensional macroporous structures with applications in a variety of disciplines from optics to catalysis. For instance, when the pore size is on the scale of the wavelength of visible light, IOs exhibit structural color due to diffraction and interference of light rather than due to absorption by pigments, making these structures valuable as nonfading paints and colorants. When IO pores are in an ordered arrangement, the IO is a 3D photonic crystal, a structure with a plethora of interesting optical properties that can be used in a multitude of applications, from sensors to lasers. IOs also have interesting fluidic properties that arise from the re-entrant geometry of the pores, making them excellent candidates for colorimetric sensors based on fluid surface tension. Metal oxide IOs, in particular, can also be photo- and thermally catalytically active due to the catalytic activity of the background matrix material or of functional nanoparticles embedded within the structure.

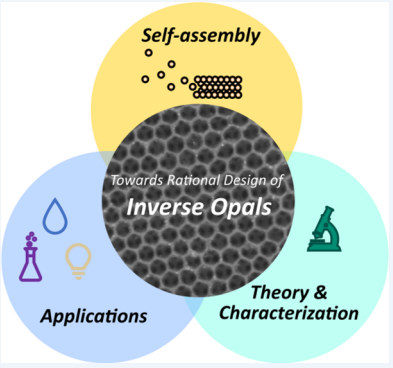

Evaporation-induced self-assembly of sacrificial particles has been developed as a scalable method for forming IOs. The pore size and shape, surface chemistry, matrix material, and the macroscopic shape of the IO, as well as the inclusion of functional components, can be designed through the choice of deposition conditions such as temperature and humidity, types and concentrations of components in the self-assembly mixture, and the postassembly processing. These parameters allow researchers to tune the optical, mechanical, and thermal transport properties of IOs for optimum functionality.

In this *Account*, we focus on experimental and theoretical studies to understand the self-assembly process and properties of metal oxide IOs without (bare) and with (hybrid) plasmonic or catalytic metal nanoparticles incorporated. Several synthetic approaches are first presented, together with a discussion of the various forces involved in the assembly process. The visualization of the deposition front with time-lapse microscopy is then discussed together with analytical theory and numerical simulations to determine the conditions needed for the deposition of a continuous IO film. Subsequently, we present high-resolution scanning electron microscopy (SEM) of assembled colloids over large areas, which provides a detailed view of the evolution of the assembly process, showing that the organization of the colloids is initially dictated by the meniscus of the evaporating suspension on the substrate, but that gradually all grains rotate to occupy the thermodynamically most favorable orientation. High-resolution 3D transmission electron microscopy (TEM) is then presented together with analysis of the wetting of the templating colloids by the matrix precursor to provide a detailed picture of the embedding of metallic nanoparticles at the pore−matrix interface. Finally, the resulting properties and applications in optics, wetting, and catalysis are discussed, concluding with an outlook on the future of self-assembled metal-oxide-based IOs.

KEY REFERENCES

- Hatton, B. D.; Mishchenko, L.; Davis, S.; Sandhage, K. H.; Aizenberg, J. Assembly of Large-Area, Highly Ordered, Crack-Free Inverse Opal Films. *PNAS* 2010, *107* (23), 10354−10359[1] - This pioneering work demonstrates a method for assembling highly ordered, crack-free inverse opal films through the coassembly of sacrificial colloidal template with a matrix material.
- Burgess, I.B.; Mishchenko, L.; Hatton, B. D.; Kolle, M.; Lončar, M.; Aizenberg, J. Encoding Complex Wettability Patterns in Chemically Functionalized 3D Photonic Crystals. *J. Am. Chem. Soc.* 2011, *133* (32), 12430−12432[2] - This work introduces an innovative technique for patterning multiple chemical functionalities into

Received: February 10, 2022
Published: June 14, 2022

https://doi.org/10.1021/acs.accounts.2c00087
Acc. Chem. Res. 2022, 55, 1809−1820

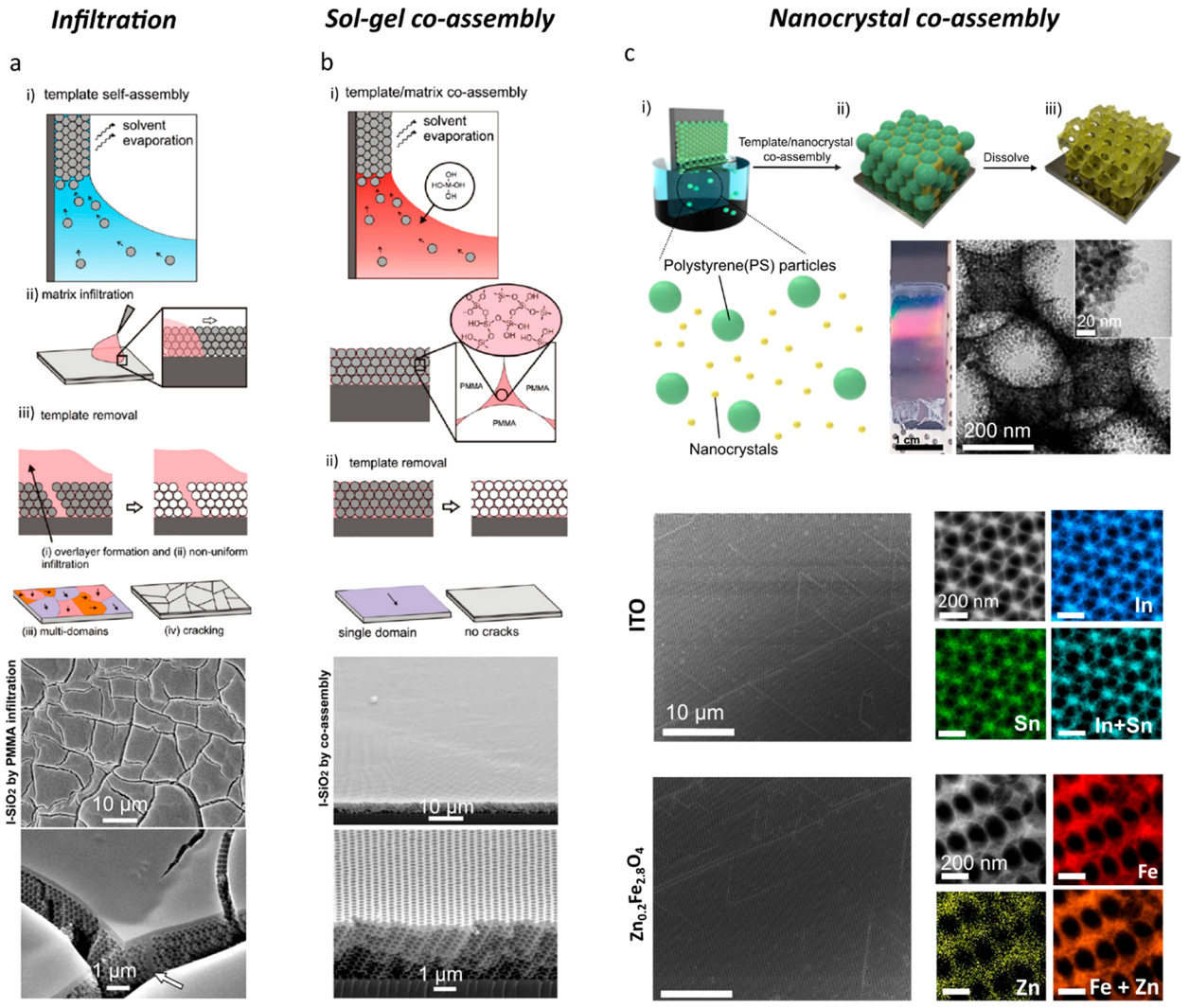

Figure 1. Evaporation-induced self-assembly routes to metal oxide inverse opals (IOs). (a) Infiltration approach. Schematic (top) and scanning electron microscope (SEM) images of the resulting cracked IO film (bottom). (b) Co-assembly using a sol−gel matrix precursor. Schematic (top) and SEM images of the resulting crack-free IO film (bottom). Images reproduced with permission from ref 1. Copyright 2010 Proc. Natl. Acad. Sci. U.S.A. (c) Co-assembly using precursor nanocrystals in the evaporating suspension. (Top, from left to right) Schematic of the approach, photograph, and transmission electron microscope (TEM) image of an IO film formed using this approach with TiO_2 nanocrystals. (Bottom) The approach demonstrated for (top row) indium tin oxide (ITO) and (bottom row) zinc iron oxide nanocrystals. SEM images of the resulting highly ordered, crack-free IOs are shown on the left with corresponding elemental mapping from energy dispersive X-ray (EDX) analysis on the right. Images reproduced with permission from ref 12. Copyright 2022 Wiley-VCH.

inverse opals for multilevel message encryption and colorimetric sensing.

- Li, L.; Goodrich, C.; Yang, H.; Phillips, K. R.; Jia, Z.; Chen, H.; Wang, L.; Zhong, J.; Liu, A.; Lu, J.; Shuai, J.; Brenner, M. P.; Spaepen, F.; Aizenberg, J. Microscopic Origins of the Crystallographically Preferred Growth in Evaporation-Induced Colloidal Crystals. *PNAS* 2021, *118* (32), e2107588118[3] - This study contributes to a new understanding of crystallographic texture development in colloidal crystals through crystallographic rotation, shedding light on the preferred ⟨110⟩ growth in the fcc colloidal crystals synthesized through evaporation-induced assembly.
- van der Hoeven, J. E. S.; Krämer, S.; Dussi, S.; Shirman, T.; Park, K. K.; Rycroft, C. H.; Bell, D. C.; Friend, C. M.; Aizenberg, J. On the Origin of Sinter-Resistance and Catalyst Accessibility in Raspberry-Colloid-Templated Catalyst Design. *Adv. Funct. Mater.* 2021, *31* (49), 2106876[4] - This study unveils that the origin of strongly enhanced nanoparticle stability in raspberry-colloid-templated (RCT) inverse opals lies in partial nanoparticle embedding in the pore−matrix interface, yielding robust and active materials for catalytic applications.

INTRODUCTION

Nature is a master at self-assembling hierarchically structured multifunctional materials, inspiring the development of synthetic analogs that mimic certain features of the complicated natural systems. These simplified synthetic materials allow researchers to vary one parameter at a time, unraveling the forces governing the assembly process and bringing us closer to the rational design of self-assembly routes toward hierarchical and multifunctional architectures. Key tools in understanding these processes are controlled assembly experiments, structural

https://doi.org/10.1021/acs.accounts.2c00087
Acc. Chem. Res. 2022, 55, 1809−1820

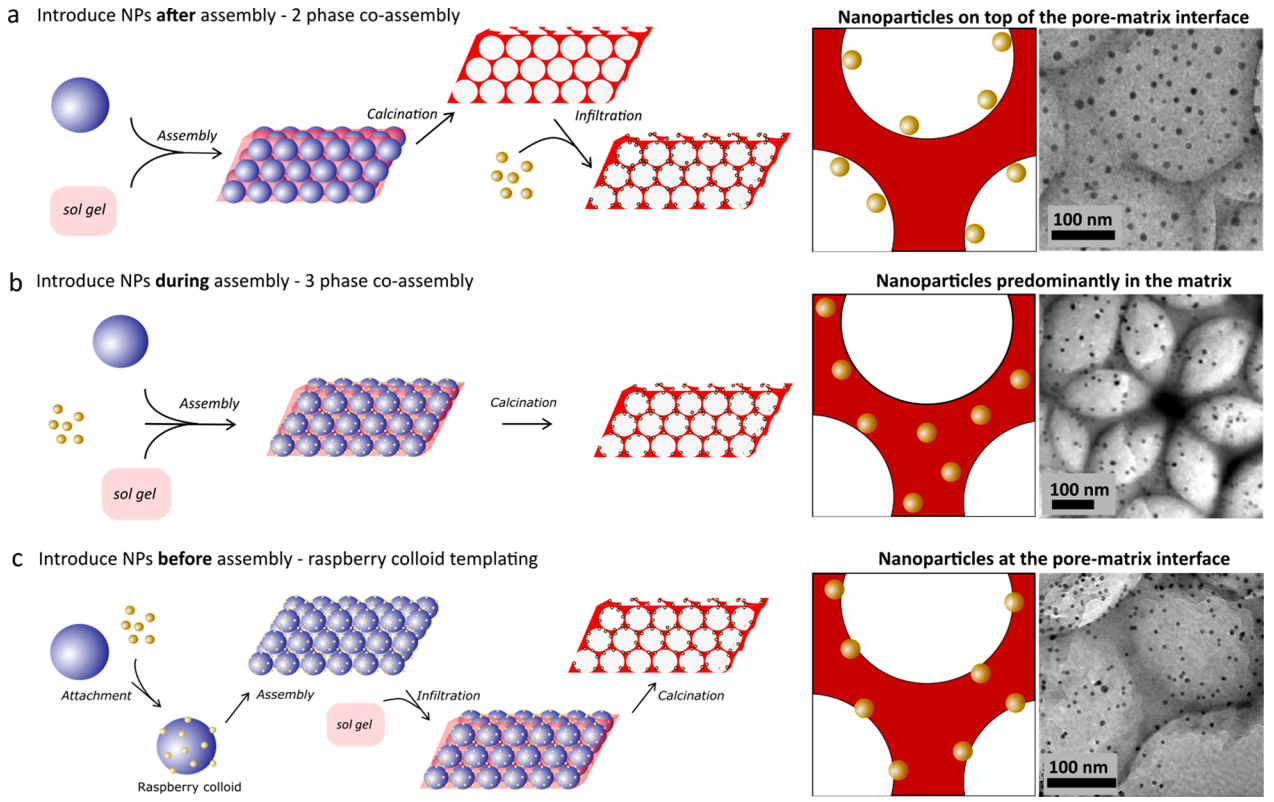

Figure 2. Incorporation of functional nanoparticles (NPs) into IOs. Introducing NPs (a) after formation of the IO, or, (b) during, or (c) before assembly of the templating colloids results in IOs with the NPs (a) in the pores, on top of the pore−matrix interface, (b) predominantly encapsulated in the matrix, or (c) embedded at the pore−matrix interface. The TEM images in panels (a) and (b) are reproduced from refs 20 and 23, respectively. Copyright 2019 and 2014 American Chemical Society. The schematics are adapted with permission from ref 4. Copyright 2021 Wiley-VCH.

characterization, analytical theory, numerical simulations, and the feedback between them.

Here, we focus on inverse opal structures, bioinspired materials with the potential for a wide range of applications.[5,6] IOs are made via the self-assembly of sacrificial colloids with a diameter between 100 nm and 1 μm into a face-centered cubic (fcc) lattice. A second material is used to fill the interstitials between the assembled spheres either during or post assembly, after which the templating colloidal particles are removed, rendering an ordered, porous network. The high degree of order makes IOs valuable for fundamental studies and tractable for simulations, where a single unit cell enclosed by periodic boundary conditions represents the entire structure. Of particular interest are metal-oxide-based IOs due to both practical and functional reasons. An important practical advantage of metal-oxide-based IOs is their ease of fabrication, with the introduction of improved and new approaches for sol−gel and nanoparticle-based self-assembly.[1,6,7] The higher refractive index (n) of the oxide (e.g., $n \approx 1.46$ for silica[8] and for $n \approx 2.6$ titania[9]) compared to the air inside ($n \approx 1$) results in the scattering of light at each pore−matrix interface and makes IOs valuable for optical applications. For instance, they can serve as sensors due to the dependence of scattering on the refractive index of the fluid infiltrating the pores. Metal oxide IOs also play a role in heterogeneous catalysis, with the metal oxides providing structural support (e.g., silica) or playing an active role in the (photo)catalytic process (e.g., titania).[10−12]

Fundamental studies provide an ever-increasing insight into IOs and their formation, leading to a greater level of control over various aspects of the assembly to produce multicomponent, shape-controlled, and chemically patterned IOs, with a rapidly expanding materials toolkit and evolving applications in photonics, biomedicine, and catalysis. This Account seeks to highlight the recent developments in the synthesis, imaging, modeling, and applications of metal-oxide-based IOs with a focus on our group's work.

SYNTHESIS

Assembly of Metal Oxide Inverse Opals

The synthesis of metal-oxide-based inverse opals can be accomplished through a variety of methods, including spin-coating, sedimentation, centrifugation, evaporation of a suspension, and dip-coating.[6] Here we focus on evaporation-induced self-assembly as it can produce highly ordered structures over large length scales.[1] Typically, polystyrene or poly(methyl methacrylate) colloids are employed as templating particles because of established synthetic methods to produce submicron-sized spheres with low polydispersity, easily adjustable sizes, and high yields. These sacrificial colloids are dispersed in water either (i) without (Figure 1a) or (ii) with a precursor of the matrix material (Figure 1b,c). In the (i) assembly and infiltration approach, the precursor for the matrix material is infiltrated into the interstitials of the preformed direct opal template.[13,14] In the (ii) coassembly approach, the colloids are assembled in the presence of a matrix precursor that is typically either a sol−gel solution or a dispersion of metal oxide nanoparticles.[1,12,15] The polymeric template is then removed, often via heat treatment (calcination) at ∼500 °C, which is above the combustion temperature of the polymer. This also solidifies the background matrix through condensation in the

https://doi.org/10.1021/acs.accounts.2c00087
Acc. Chem. Res. 2022, 55, 1809−1820

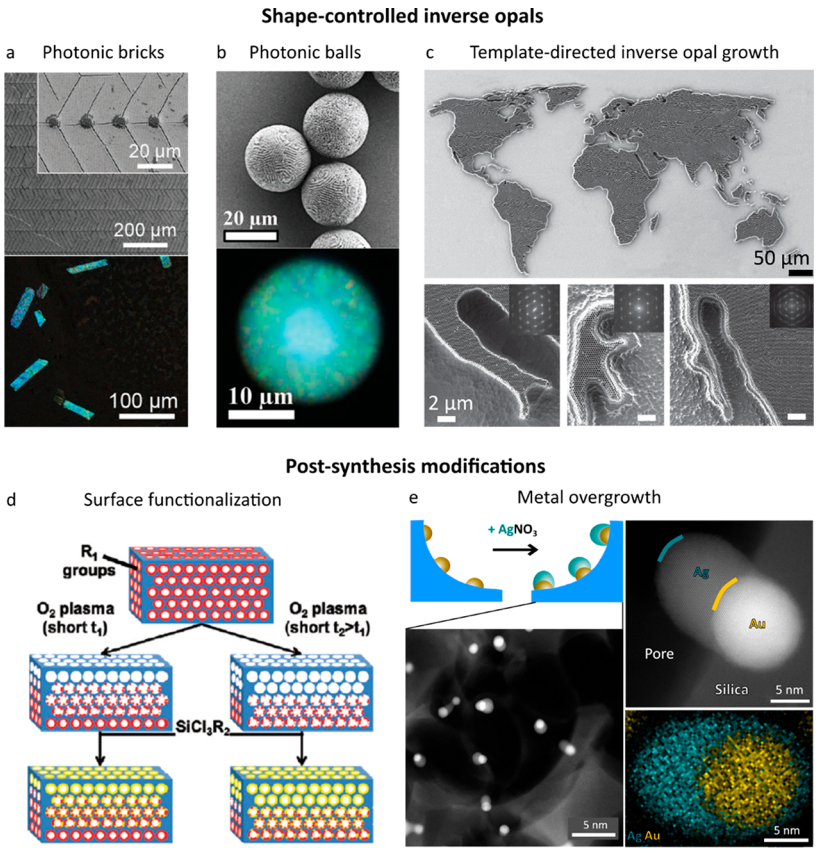

Figure 3. Control over various aspects of the assembly. (a) Photonic brick fabrication via controlled crack formation on a prepatterned surface.[18] Images reproduced with permission from ref 18. Copyright 2020 Wiley-VCH. (b) Photonic IO balls obtained via emulsion-templated self-assembly. Images reproduced with permission from ref 19. Copyright 2018 Wiley-VCH. (c) Shape-controlled inverse opals fabricated by top-down patterning of an IO film into the desired shape.[28] The bottom high-magnification SEMs and diffraction patterns of regions in the top SEM indicate high order. Images reproduced with permission from ref 28. Copyright 2015 Wiley-VCH. (d) Chemical surface modification of inverse opals: short O_2 plasma exposure between successive silane treatments of the metal oxide matrix can be used to obtain differently functionalized regions in the IO.[2,30] Schematics reproduced from ref 30. Copyright 2012 American Chemical Society. (e) Metal (Ag) overgrowth on embedded Au NPs. The high-angle annular dark field−scanning transmission electron microscopy (HAADF-STEM) images and EDX maps show anisotropic Ag shell growth, resulting in Janus-like NPs.[4] Images reproduced with permission from ref 4. Copyright 2021 Wiley-VCH.

case of a sol−gel precursor or by promoting sintering for a nanocrystalline precursor. Calcination can be used to manipulate the shape of the pores, with temperatures above the glass transition of the matrix (800−1100 °C for SiO_2), inducing the formation of elliptical voids as the matrix deforms under its own weight.[16,17] If the IO is deposited on a temperature-sensitive substrate such as a conductive or flexible polymer or if the crystal structure or polymorph of the temperature-sensitive metal oxide matrix must be preserved for intended functionality, wet-chemical approaches relying on the dissolution of the templating particles in an organic solvent can be applied instead. A low-temperature pretreatment (e.g., ≤ 200 °C) may be required to solidify the metal oxide matrix preventing its collapse upon dissolution of the templating colloids.[12]

In all cases, a high degree of order relies on: (i) low polydispersity of the colloidal particles (<10%); (ii) sufficiently repulsive interactions between all assembling components to prevent uncontrolled aggregation that results from van der Waals attraction; and (iii) solvent evaporation rate that is high enough to ensure that the time scale of deposition exceeds that of sedimentation but slow enough to allow the colloids to move into a crystalline lattice position rather than being kinetically trapped in a disordered state. The characteristics of the precursor are also essential, especially in the case for coassembly. For example, the evaporation rate should exceed the condensation rate for a sol−gel precursor.

Choice of Assembly Route

An advantage of the infiltration approach (Figure 1a) is that it can easily be adjusted to fabricate IOs for a wide range of metal oxide materials: as the colloidal crystal is formed first, interactions between the colloid and matrix material do not affect the self-assembly. However, cracks are more prevalent using this approach due to capillary forces that pull the matrix precursor into the interstices of the direct opal, whereas in coassembly, the templating colloids can shift their location in the gelled partially hydrolyzed sol or in the colloidal suspension, mitigating tensile stresses between the shrinking colloidal crystal and rigid substrate.[1] Voids and irregularly shaped pores can also result in the infiltration approach if the infiltrating matrix material does not adequately wet the surface of the templating colloids. A challenge of sol−gel-based coassembly, however, is its high sensitivity to the metal oxide precursor composition, specifically its associated charge, hydrolysis and condensation rates, and degree of shrinkage upon drying. For instance, cracking in TiO_2-containing sol gels is much more pronounced than in their SiO_2 counterparts due to an ∼2× greater shrinkage of the tested TiO_2 sols compared to SiO_2 sols.[18] This sensitivity to the precursor can be addressed by employing presynthesized

https://doi.org/10.1021/acs.accounts.2c00087
Acc. Chem. Res. 2022, 55, 1809−1820

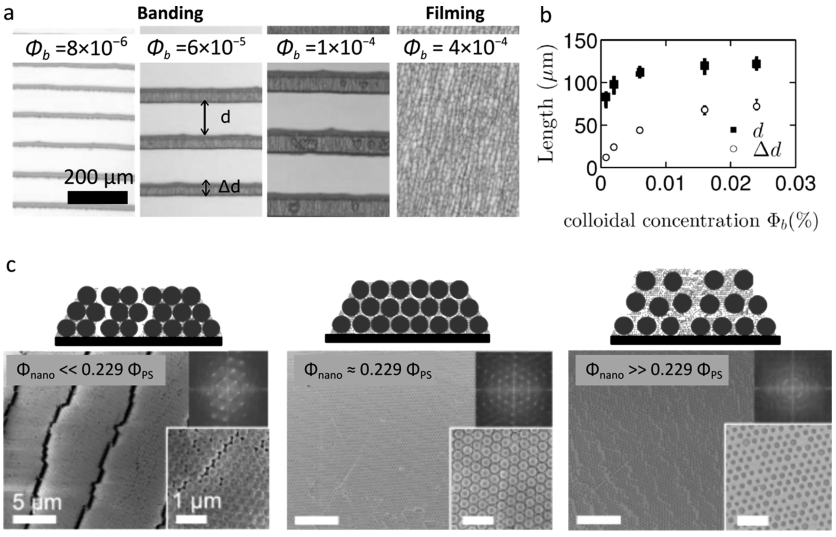

Figure 4. Drying effects in evaporative self-assembly. (a,b) Banding vs filming: Micrographs of periodic bands and uniform films of colloidal deposits (a) and band spacing d (■) and bandwidth Δd (°) as a function of the colloidal volume fraction φ_b (b). Images adapted with permission from ref 34. Copyright 2015 American Institute of Physics. (c) SEM images of compound opal structures at different ϕ_{nano}/ϕ_{PS}. Bottom insets are zoom-ins to show the packing, while the top inset shows the diffraction pattern. Images adapted with permission from ref 12. Copyright 2022 Wiley-VCH.

metal oxide nanocrystals with sufficient surface charge originating from the ligands on the nanocrystals surface. This allows the fabrication of a range of metal oxide IOs without having to change the assembly conditions, as demonstrated for titania, alumina, zirconia, indium tin oxide, and zinc iron oxide (Figure 1c).[12,15]

Hybrid Inverse Opals with Metal Nanoparticles

The functional properties of IOs can be expanded by incorporating various nanoparticles (NPs) into the metal oxide framework, such as those with plasmonic or catalytic properties. NPs can be introduced at different stages: (i) after the IO has been formed (Figure 2a), or (ii) during (Figure 2b) or (iii) before (Figure 2c) the assembly of the templating colloids, which results in their placement (i) on top of the pore−matrix interface, (ii) mostly encapsulated in the metal oxide matrix, or (iii) partially embedded at the pore−matrix interface.[19] Briefly, (i) involves infiltrating a NP solution into an already-formed IO[20−22] and (ii) is a three-phase coassembly in which functional NPs are added as a third phase to the coassembly mixture.[23] The raspberry colloid templating (RCT) approach (iii) entails first synthesizing NPs and attaching them to the templating colloids and then adding these hybrid "raspberry" colloids to the evaporating suspension to produce metal-oxide IOs with NPs exclusively located at the pore−matrix interface but largely embedded into the matrix compared to the NPs attached to the interface, as in (i).[4,19] A unique feature of the RCT materials is the sinter-resistance of the metal NPs at elevated temperatures and in reactive gases,[4,20,24] making them valuable materials for thermal catalytic applications as detailed further in the Imaging and Modeling and Applications sections.

Varying the Macroscopic Structure of the IO

In addition to the choice of composition, incorporated particles, and pore structure, the macroscopic properties of IOs can be imposed using one of the following approaches: (i) deposition on a substrate that is patterned,[18] curved,[25] flexible, or made with a sacrificial material that allows for release of brick-like IOs (Figure 3a);[18] (ii) assembly in confinement, for example, in emulsion-based liquid droplets (Figure 3b);[19,25,26] (iii) 3D printing of the suspension;[27] and (iv) photo- or electron-beam lithography to create a mask above an already-formed IO on a substrate followed by reactive ion etching (Figure 3c).[28,29] The imposed curvature or pattern of a substrate affects the order of the resulting colloidal crystal, where substrates with smaller radii of curvature result in IOs that deviate more from perfectly ordered crystals.[18] In the case of spherical confinement, photonic balls are most ordered at the surface and become progressively more disordered toward the center.[25]

Postsynthesis Modifications

IOs can be modified after their synthesis in a variety of ways in addition to the top-down patterning presented in Figure 3c. The surface can be chemically functionalized (Figure 3d), generally achieved through the addition of a silane monolayer by vapor- or solution-phase deposition on the metal oxide surface, homogeneously or in a predefined pattern.[30] Two or more distinct surface chemistries can be created across the IO by using a combination of masking (e.g., with polydimethylsiloxane (PDMS)) and oxygen plasma etching, which removes any silane molecules in regions which have been exposed. The IO can be subsequently functionalized with a new silane.[2,30] Vertical gradients in the surface chemistry are also possible by exposing the IO to plasma for a shorter time to partially clean the first silane off the surface, with more removal occurring in the uppermost layer of pores.[31] When a second silane is introduced, it only attaches to the cleaned sections (Figure 3d). A surface chemical gradient across an IO can also be accomplished by codepositing two silanes at differing concentrations.[32]

Likewise, metal overgrowth can be applied to functional NPs in hybrid IOs to produce larger nanoparticles or those consisting of multiple metals (Figure 3e). Metal overgrowth can be used to modify the optical[4,23] and catalytic properties of the NPs in hybrid IOs and typically involves infiltrating the IO with metal precursor solution (e.g., $HAuCl_4$ for gold[23] or $AgNO_3$ for silver[4]), followed by the addition of a mild reducing agent. Preferential growth in the direction of the void due to spatial- and mass transfer limitations at the embedded sides of the NPs results in the characteristic elongated shape of the overgrown NPs (Figure 3e).

https://doi.org/10.1021/acs.accounts.2c00087
Acc. Chem. Res. 2022, 55, 1809−1820

MECHANISTIC STUDIES: IMAGING AND MODELING

Drying Dynamics

During self-assembly, the meniscus of a drying suspension is pinned to a substrate or the walls of the container, and fluid flows into the region of the meniscus to compensate for fluid lost due to evaporation.[33] This drives the colloids and precursor (if present) to the contact line, where they subsequently form a wet solid at the interface, as seen in the coffee ring effect. During this process, the meniscus deforms as a function of the local particle deposition and evaporation rates. Depending on whether or not the meniscus touches down onto the substrate, the particle packing can span a continuous solid film or can be arranged in periodically spaced bands, as shown in Figure 4a. An in-depth study of the deposition process combining experiments and theory by Kaplan et al. provided an understanding of the regimes in which filming versus banding could be expected.[34] It was determined that a continuous film forms when the bulk volume fraction of particles, φ_b, is above a critical concentration, φ_c. Periodically spaced bands are formed for $\varphi_b < \varphi_c$, with the thickness of the bands decreasing with decreasing φ_b (Figure 4a). A coarse-grained description capturing the dynamics of meniscus deformation revealed that φ_c is the volume fraction for which the rate of colloid deposition equals the rate of solvent evaporation. The spacing between bands (d) can be predicted for a given particle volume fraction and evaporation rate. A more detailed multiphase model that couples the inhomogeneous evaporation at the meniscus to the fluid flow and particle advection was developed to enable the quantification of the minimum deposition rate required to achieve a continuous film for a given evaporation rate, the thickness of bands in the banding regime (Δd), and the critical volume fraction at which the transition from one mode of deposition to the other occurs, all of which match nicely with the experimental findings (Figure 4b).

When nanocrystals are introduced into the coassembly mixture, it is important that their concentration relative to that of the colloids is appropriate for the assembly into ordered crack-free IO films. Matching the constitutive fluxes of both types of particles as prescribed by the packing geometry of a modified *fcc* lattice and accounting for the denser packing of the bulk of the crystal compared to the bottom substrate-anchored layer, Han et al.[12] calculated the theoretical value of the optimal volume fraction ratio of nanocrystal matrix precursor to templating colloids, $\left(\frac{\phi_{nano}}{\phi_{PS}}\right)^*$, to be ~0.023. This value was experimentally validated to produce crack-free IOs across several nanocrystalline metal oxide precursors, whereas cracked IOs with underfilled interstitials or crack-free IOs with disordered arrangement of voids were produced for $\left(\frac{\phi_{nano}}{\phi_{PS}}\right)$ well below or well above this critical value, respectively (Figure 4c).

Crystal Structure of Crack-Free IOs

Evaporation-induced coassembly on vertically oriented substrates results in colloidal crystals with a preferred growth along the ⟨110⟩ direction. This phenomenon appears general and has been observed for a variety of colloid chemistries, evaporation rates, and matrix precursors.[1,3,12,18] The origin of the preferred crystallographic growth orientation during coassembly has recently been elucidated by Li et al. through analysis of the local organization of colloidal crystals at different growth stages using a combination of two-dimensional large-area crystallographic mapping and crystal structure analysis at a single-particle level by high-resolution SEM imaging, together with finite element-based mechanical simulation and computational colloidal assembly modeling.[3] This multipronged approach unveiled that the assembly process proceeds in 3 stages: (i) nucleation of a polycrystalline colloidal monolayer along the horizontal meniscus direction M (Figure 5), (ii) increase of the number of layers depending on colloidal concentration; and (iii) gradual rotation of the grains in the multilayered colloidal crystal until the close-packed direction coaligns with the growth direction G, after which the assembled cm-sized film remains uniformly ⟨110⟩-oriented. The rotation toward the ⟨110⟩ direction of the individual grains occurs regardless of their initial crystal orientations. Geometrically necessary dislocations (GNDs) are essential in facilitating the rotation; they arise due to drying-induced mechanical stress that results from a mismatch between the shrinkage of the colloidal crystal film

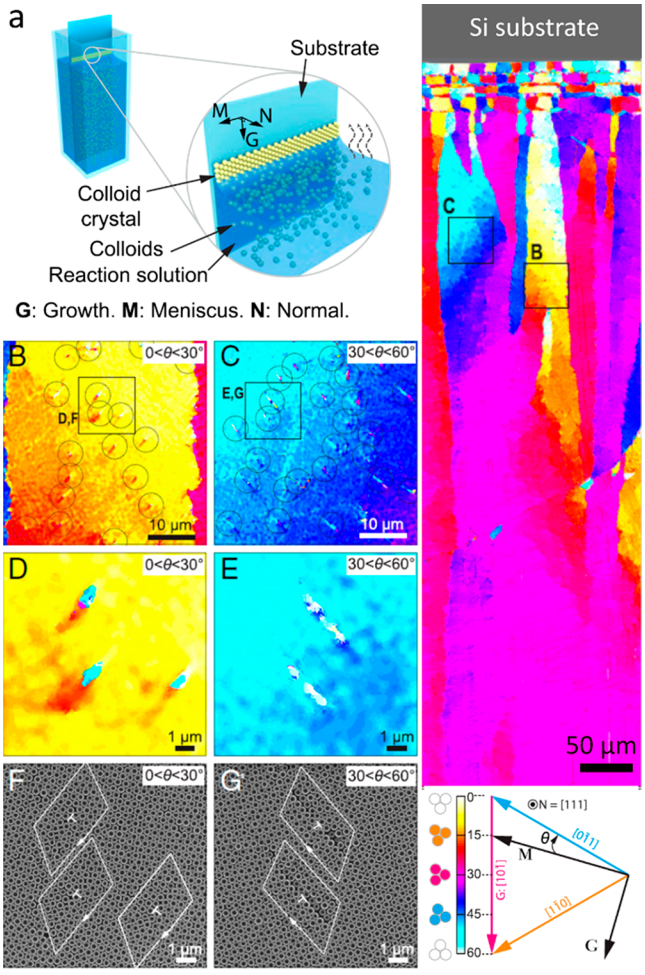

Figure 5. Evolution of the crystallographic direction of colloidal crystals upon evaporation-induced coassembly. (a) Schematic of the process and a large-area map of the crystallographic orientation demonstrating its gradual rotation along the growth direction. (b,c) High-magnification of the square regions from panel (a), with local crystal orientation relative to the meniscus direction (θ) indicated. The circles highlight individual GND defects. (d,e) High-magnification of the boxes regions in panels (b,c). (f,g) Original SEM images for panels (d,e), showing the individual GNDs. Images adapted with permission from ref 3. Copyright 2021 Proc. Natl. Acad. Sci. U.S.A.

https://doi.org/10.1021/acs.accounts.2c00087
Acc. Chem. Res. 2022, 55, 1809−1820

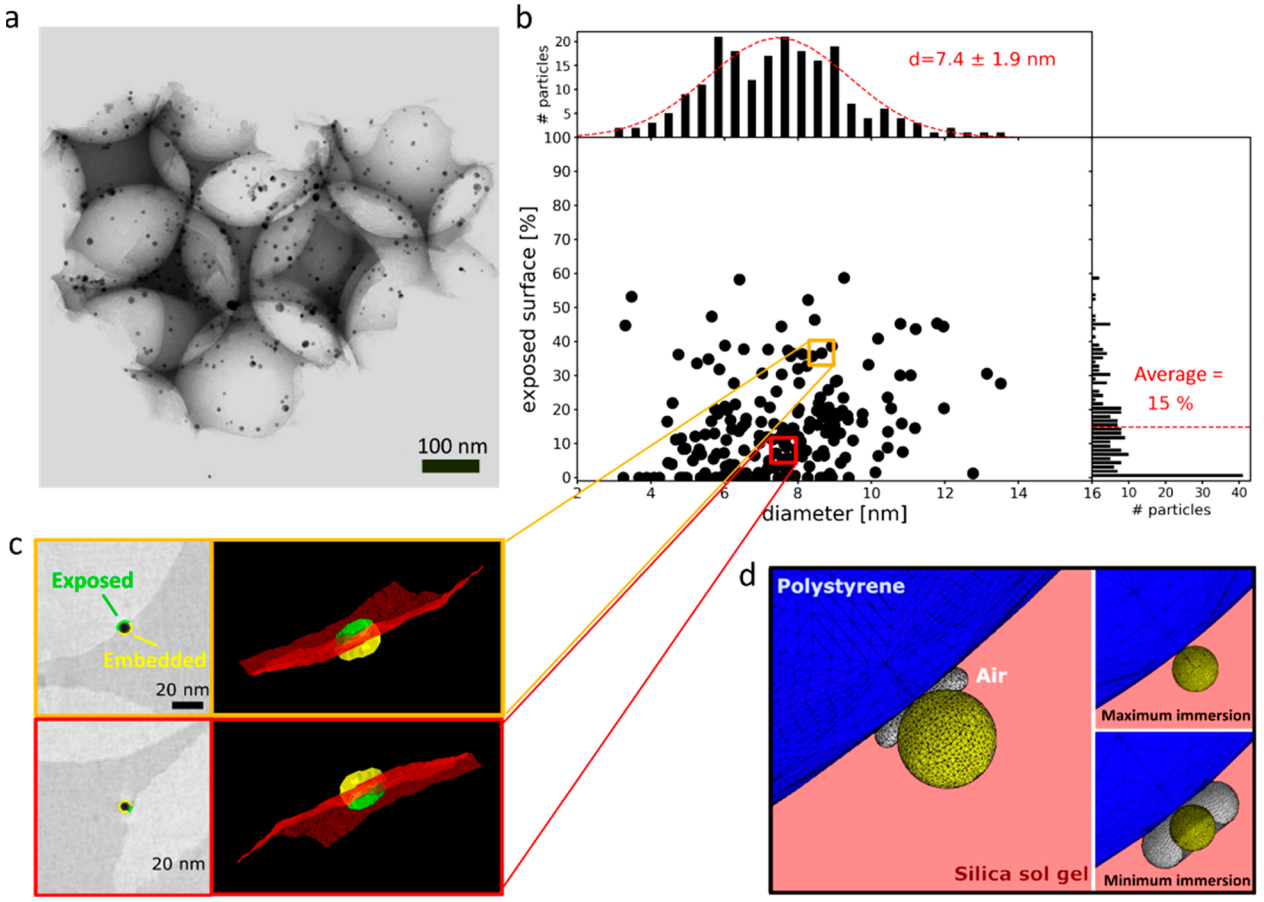

Figure 6. Quantification and modeling of the nanoparticle embedding in raspberry-colloid-templated (RCT) inverse opals. (a) Bright field TEM of a silica-based RCT IO containing $Au_{96}Pd_4$ metal nanoparticles. (b) Plot of the exposed nanoparticle surface as a function of particle diameter (middle graph) determined from the 3D electron microscopy data. Histograms show the particle size distribution (top) and the exposed surface distribution (right). (c) Examples of two NPs with measured 64% (top) and 93% (bottom) of the surface embedded into matrix. (d) Numerical calculations show the equilibrium state silica sol−gel solution−air contact line at the NP−polystyrene interface, with larger trapped air bubbles leading to a lower degree of immersion in the sol−gel. The snapshots on the right depict numerical calculations of two extreme cases of maximum (∼100%) and minimum (∼30%) embedding. Images reproduced with permission from ref 4. Copyright 2021 Wiley-VCH.

and the constraint from the rigid substrate during the drying process. As mechanical stresses are often present in evaporating systems, it is likely that the mechanical stress-induced dislocations and the corresponding rotation of the crystal grains in coassembled colloidal crystals are a universal principle for crystallographically preferred growth in evaporation-induced colloidal assemblies and the corresponding IOs. This phenomenon depends on the thickness of the colloidal crystal and holds for thin films, whereas cracking becomes the strain release mechanism for thicker films. The thickness at which this transition occurs depends on the shrinkage of the sol−gel material. For example, in silica sol−gel films produced with 250−400 nm templating colloids, the threshold is approximately 20 layers, whereas for mixed titania-silica sol−gels that shrink more, the threshold is lower.[35]

Nanoparticle Embedding

As mentioned in the Synthesis section, the nanoparticle placement in hybrid IOs can be controlled via the assembly process.[20,21,23,36] Van der Hoeven et al.[4] recently employed high-resolution 3D transmission electron microscopy (TEM) together with numerical simulations to gain insight into the observed benefits of RCT IOs, such as sinter- and mechanical resistance. Quantitative assessments of >200 individual AuNPs revealed that all NPs reside at the pore wall, with >50% of their surface embedded in the silica matrix (Figure 6a−c). The degree of embedding was shown to largely depend on the wetting behavior of the precursor used to infiltrate the assembled raspberry colloids. The measured contact angles, which a sol−gel silica solution forms on gold and polystyrene surfaces, were used to numerically calculate the shape of the solid−liquid−vapor contact line that forms a stable sol−gel interface between the gold NPs and the polystyrene colloid (Figure 6d). The calculations revealed that the largest captured air volume that can stabilize the contact line would lead to a minimum 30% nanoparticle immersion into the sol−gel solution, and thus all NPs must be largely embedded into the matrix material, in agreement with high-resolution TEM results. The wetting behavior of the sol−gel solution on the raspberry colloids, and consequently the nanoparticle embedding into the oxide, can be varied by changing the composition of the sol−gel solution or by functionalizing the raspberry colloids with hydrophobic or hydrophilic ligands. Gaining such control over the nanoparticle embedding would enable one to vary the nanoparticle stability and nanoparticle accessibility. This is particularly relevant for applications in heterogeneous catalysis where the nanoparticle-support interaction is known to be a key parameter in tuning the catalytic performance, and similar control cannot be accomplished using conventional catalyst preparation techniques.

https://doi.org/10.1021/acs.accounts.2c00087
Acc. Chem. Res. 2022, 55, 1809−1820

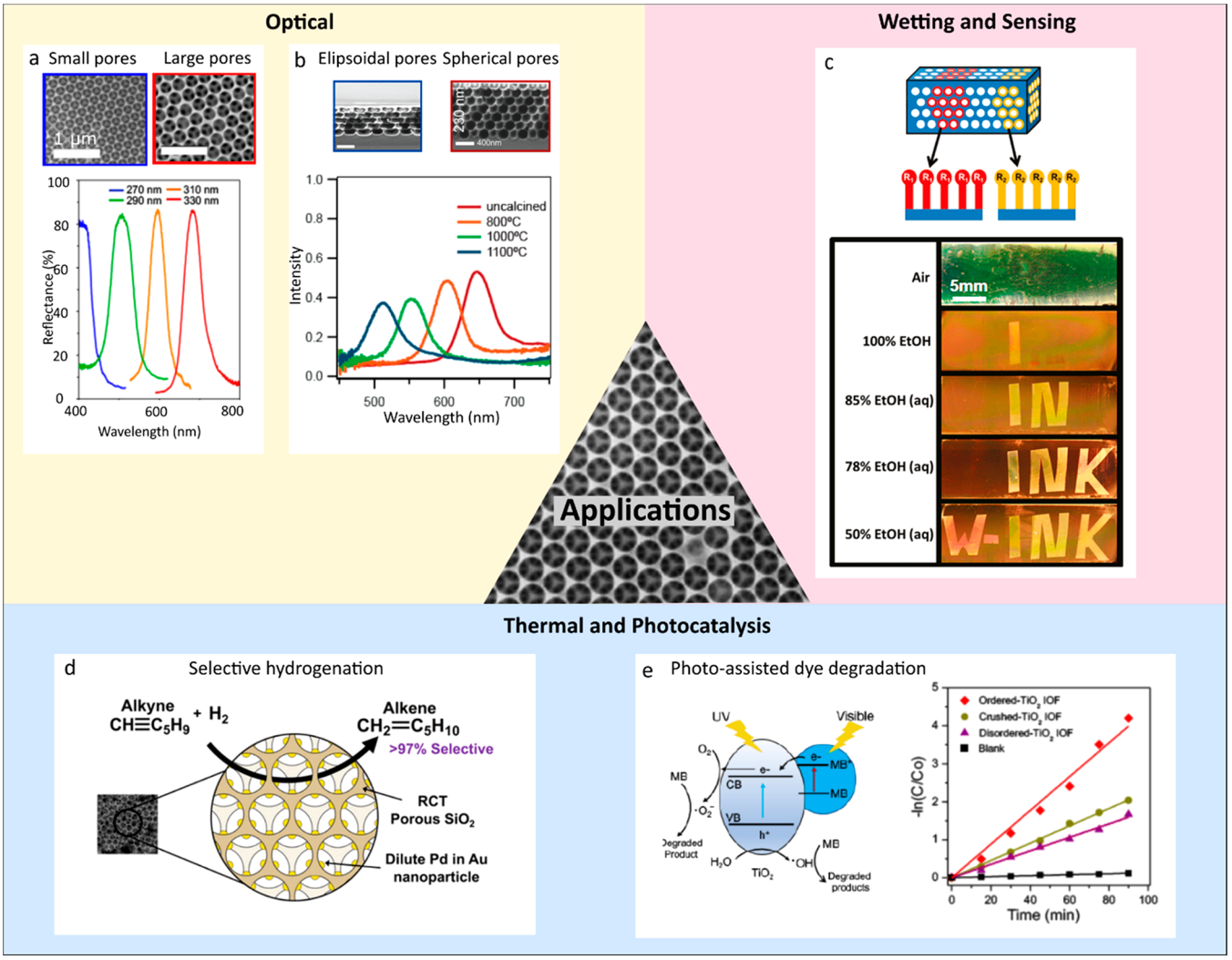

Figure 7. Optical, wetting, sensing, and catalytic applications of inverse opals. (a) Reflectance spectra of TiO_2 IOs templated by colloids of different sizes.[12] Images adapted with permission from ref 12. Copyright 2022 Wiley-VCH. (b) Optical spectra of a single sample with progressively more elliptical voids, due to calcination at sequentially higher temperatures.[16] Images reproduced from ref 16. Copyright 2014 American Chemical Society. (c) Schematic and optical images showing a chemically encoded IO functioning as a colorimetric sensor in which the word "W-INK" is encoded by progressively hydrophobic surface functional groups.[2] In different water-ethanol mixtures, different words appear. Images reproduced from ref 2. Copyright 2011 American Chemical Society. (d) Thermal catalysis with RCT materials containing gold-palladium nanoparticles for the selective hydrogenation of alkynes to alkenes.[44] Images reproduced from ref 44. Copyright 2020 American Chemical Society. (e) Photoassisted dye degradation of methylene blue using TiO_2 inverse opals. Ordered IOs outperform their crushed and disordered counterparts.[12] Images reproduced with permission from ref 12. Copyright 2022 Wiley-VCH.

APPLICATIONS

Optical Applications

Inverse opals with pore sizes on the length scale of visible wavelengths display structural color, whose wavelength and angle-dependence can be designed through the choice of the refractive index of the materials, void size and shape, lattice structure, and degree of order.[5] The observed color shifts to longer wavelengths for IOs created with progressively larger templating colloid sizes (Figure 7a). A narrow peak and large intensity of the reflection spectrum indicate that the refractive index is organized in a periodic pattern.[12] Elliptical voids change the length scale of the patterning of the refractive index as well as the lattice symmetry, which affects the observed color and its angle-dependence (Figure 7b).[16] Another way to affect the angle-dependence of the color is increasing the deviation of the lattice from perfect order, for example through the addition of salts or increase in polydispersity of templating colloids in the assembly solution. Increased disorder results in less color-travel.[37−39] Meanwhile, the color purity of IOs can be enhanced by forming them on a substrate which absorbs visible light such as a silicon wafer or by including broadband or narrowband absorbers, such as carbon black or plasmonic particles, respectively, within the IO.[40]

Ordered IOs are particularly interesting as they are 3D photonic crystals, structures with a periodically patterned refractive index that have been of great interest to the nanophotonics community.[5,14,41] Beyond their use as "structural pigments," photonic crystals provide a wealth of exciting opportunities in applications involving light, such as acting as mirrors for a specific wavelength range, which is useful to make filters, beamsplitters, waveguides, and lasers.[41] Photonic crystals can also enhance light-matter interaction for certain wavelengths due to the so-called "slow-light effect," where the exact

https://doi.org/10.1021/acs.accounts.2c00087
Acc. Chem. Res. 2022, 55, 1809−1820

wavelength can be designed through the choice of template size and refractive indices of the background material and fluid in the voids.[42] Researchers have employed this phenomenon to create IO-based photovoltaics/solar cells and photocatalysts with a high absorption of light by the IO background material, functional NPs included in the IO, or molecules dissolved in the infiltrating fluid.[10−12,43]

The use of IOs is not limited to visible wavelengths. When void sizes are much larger or smaller than the ones necessary for coherent scattering of visible light, they can produce identical effects in the ultraviolet or infrared wavelengths, respectively. Furthermore, an IO will appear as an effective medium to incoming light whose wavelength exceeds the IO pore size, meaning that the IO can be treated as a bulk material with effective refractive index given by the sum of the refractive indices of the background matrix material and that of the fluid in the voids. Using this principle, Shahsafi et al. demonstrated that an SiO_2 IO with ∼300 nm pores acts as a near-perfect absorber with very low angle-dependence for specific wavelengths in the mid-infrared (∼9 μm). This is a hard-to-obtain and desirable characteristic for a variety of devices, such as those that can direct the thermal emission of materials, and for highly sensitive sensors in the mid-infrared.[45]

Wetting, Sensing, and Biomedical Applications

The re-entrant geometry of the openings between the spherical voids of an IO creates an energy barrier to fluid infiltration, such that a liquid will pass from one pore to another only if its contact angle is below a threshold value, determined by the opening angle and the chemical functionalization of the pore surface; otherwise, the liquid will remain in the metastable nonwetted state, pinned above an air-filled pore. When fluid fills the pores, the absolute refractive index increases while the refractive index contrast typically decreases, causing a redshift and dimming of the color, respectively. These changes can be monitored by eye or spectroscopically, making IOs valuable as colorimetric sensors based on fluid surface tension that is limited in resolution only by the uniformity of the surface coating and the neck angles across the IO.[30,46]

Patterning the surface chemistry of an IO results in multiple critical wetting thresholds across the structure, so that fluids with distinct surface tensions produce different filling patterns. This concept has enabled the differentiation of test liquids (Figure 7c,d).[2,30,32] Vertical gradients in surface chemistry (Figure 3d) result in partial wetting into the structure, which is especially useful for biomedical applications, as was applied to the detection of bile salts in the urine of infants with neonatal jaundice.[31] More targeted IO diagnostic sensors can use antibodies bound to the surface to capture viral particles, leading to small but measurable spectral shifts in the IO peak reflectance.[47] The IOs can also be functionalized with molecules that shift their wetting characteristics in response to outside stimuli. For example, IOs coated with photoswitchable azobenzene molecules serve as cumulative detectors of exposure to elevated temperature or UV dose, as azobenzene degradation due to heat or photobleaching, respectively, reduces the IO surface energy.[2,48] Such IOs can be used as effective antitampering or quality-control sensors. In addition to static sensing of surface tension, the dynamics of wetting and/or drying can be used to enhance the distinction between otherwise similar solvents.[49]

The textured surface of IOs functionalized with hydrophobic molecules can also be used as a superhydrophobic material. By infusing lubricant into IOs, an omniphobic surface with low contact angle hysteresis is created.[50,51] This fits well within the family of slippery liquid-infused porous surface (SLIPS) materials,[52] which show exceptional antifouling properties due to their ability to repel any contaminating substances, including ice, blood, and bacteria.[53] The reentrant curvature of the IO pore openings firmly locks the lubricant within the structure, resulting in robust omniphobicity that prevails even after the application of strong shear forces and mechanical damage. Structural color of these IOs can also act as a reporter for lubricant depletion.[54,55] IO SLIPS coatings on various condensation surfaces such as copper pipes in heat exchangers prevent droplet pinning for improved heat transfer and exhibit only minute losses of lubricant, as measured by Adera et al.[56]

Catalytic and Photocatalytic Applications

Metal nanoparticles supported on a metal oxide are widely used in chemical industry as heterogeneous catalysts to accelerate chemical reactions. Hybrid IOs are promising materials for fundamental catalysis studies regarding structure-performance relations[57−59] and for more applied studies under industrially relevant conditions.[24] Key advantages of IOs for catalysis are (i) a highly interconnected porous network, facilitating mass-transport,[60] (ii) well-dispersed and highly accessible catalytic nanoparticles especially in the RCT approach, and (iii) a large design space for the composition, size, and shape of the metal nanoparticles and metal oxide, therefore allowing a targeted design to match specific chemical reactions.[19] So far, the catalytic performance of well-defined mono- and bimetallic Au, Pd, Pt, and Ag nanoparticles on silica and alumina RCT materials have been investigated for selective oxidation and hydrogenation reactions (Figure 7e).[20,24,44,57,61] Furthermore, mono- and bimetallic Pd-based RCTs were used as oxidation catalysts for CO[20,24] and volatile organic compounds at lower temperatures compared to their commercial counterparts and at significantly reduced metal loadings.[24] A common problem of commercial catalysts performing at high temperatures and/or high air flows is that the NPs can migrate and sinter or leach, which reduces the activity of the catalyst. The RCT design suppresses NP sintering due to the embedding of the nanoparticles in the metal oxide support,[4,24] which we have shown for a variety of RCT compositions. For example, TEM measurements revealed minimal NP growth after thermal treatment at 800 °C (e.g., AuPd NPs[4]) and 950 °C (e.g., Pd NPs[4,24]), whereas their nonembedded inverse opal counterparts (prepared by infiltration post assembly) already sintered severely upon thermal treatment at 500 °C.[20]

IOs are also of great interest for photocatalysis due to their high active surface area, as well as the relatively thin metal oxide walls, providing a short distance for reactive electrons or holes to travel to the interface where they can reduce or oxidize reactants. TiO_2 IOs are one of the most commonly employed IOs in photocatalytic applications as TiO_2 has a relatively high refractive index,[10,12] which leads to strong light scattering even when the pores are infiltrated with liquid. The performance can be enhanced by the slow-light effect, which is an increase in light-matter interaction time arising from the specific choice of pore size and materials composition.[10,42] The slow-light effect has been studied for a variety of systems, including for photo-degradation of methylene blue by varying the degree of order in the IOs, where the ordered IOs outperformed the more disordered structures when illuminated with light of the expected wavelength for the slow-light effect (Figure 7f).[10,12]

https://doi.org/10.1021/acs.accounts.2c00087
Acc. Chem. Res. 2022, 55, 1809−1820

CONCLUSIONS AND FUTURE PERSPECTIVES

This Account is focused on the synthesis, fundamental understanding, and applications of metal-oxide inverse opals produced by evaporation-induced self-assembly. The modularity of the self-assembly approach allows researchers to create a variety of IOs composed of different materials, with tailored chemical functionalization, patterning, functional nanoparticle incorporation, pore structure, overall geometry and order of the IO, and the substrates on which they are deposited. These aspects, in turn, influence the IO's physical and chemical properties, which can be critical to applications. Herein, we discussed the mechanistic underpinnings of the evaporation and deposition dynamics required for ordered assembly over large length scales, the development of crystallographically oriented IO films due to geometrically necessary dislocations, unique wettability of IOs due to the re-entrant geometry of the porous network, and the dependence of the NP placement within the IO matrix on the wetting of the solution for the raspberry-colloid-templated approach. Insights from these studies can be applied directly to improving our understanding of and control over the assembly process and to produce better-quality structures targeted to specific end-uses. A greater control over crystallographic defects during the assembly process would be particularly valuable for guiding the flow of light. Optical cavities in IOs could be combined with a gain or absorbing medium to produce lasers or photovoltaics, respectively. As the condition for light confinement in such cavities is highly sensitive to the local refractive index, there are many opportunities to further explore and develop IOs with controlled defects to sense minute changes in the refractive index for biomedical applications. Chemically functionalized IOs are excellent candidates for colorimetric sensing. Changes to the metal oxide could be explored, such as adding dopants to create electrically conductive IOs, which could be incorporated into next-generation batteries and fuel cells. The development of IOs for catalytic applications is an exciting direction, where the structural characteristics of the raspberry-colloid-templated IOs are particularly promising due to the unique partial nanoparticle embedding and resulting sinter-resistance under harsh catalytic conditions. We expect that new metal and metal-oxide combinations open a wider range of applications in gas- and liquid-phase catalysis and electrochemical applications.

AUTHOR INFORMATION

Corresponding Author

Joanna Aizenberg − *Harvard John A. Paulson School of Engineering and Applied Sciences, Harvard University, Cambridge, Massachusetts 02138, United States; Department of Chemistry and Chemical Biology, Harvard University, Cambridge, Massachusetts 02138, United States;* orcid.org/0000-0002-2343-8705; Email: jaiz@seas.harvard.edu

Authors

Jessi E.S. van der Hoeven − *Harvard John A. Paulson School of Engineering and Applied Sciences, Harvard University, Cambridge, Massachusetts 02138, United States; Department of Chemistry and Chemical Biology, Harvard University, Cambridge, Massachusetts 02138, United States; Materials Chemistry and Catalysis, Debye Institute for Nanomaterials Science, Utrecht University, 3584 CG Utrecht, The Netherlands;* orcid.org/0000-0001-9832-289X

Anna V. Shneidman − *Harvard John A. Paulson School of Engineering and Applied Sciences, Harvard University, Cambridge, Massachusetts 02138, United States*

Natalie J. Nicolas − *Harvard John A. Paulson School of Engineering and Applied Sciences, Harvard University, Cambridge, Massachusetts 02138, United States*

Complete contact information is available at: https://pubs.acs.org/10.1021/acs.accounts.2c00087

Author Contributions

‖These authors contributed equally

Notes

The authors declare no competing financial interest.

Biographies

Jessi E.S. van der Hoeven received her Ph.D. in Chemistry at Utrecht University on the topic of gold nanorod synthesis for sensing and catalysis. She then studied inverse opal catalysts at Harvard University, and is now an assistant professor at Utrecht University, focusing on electron microscopy for catalytic materials.

Anna V. Shneidman received her Ph.D. in Chemical Physics at Harvard University on the topic of nanoscale optics. She is now a research associate at Harvard, focused on self-assembly and light-matter interactions in a variety of bioinspired materials.

Natalie J. Nicolas is a Ph.D. candidate in Materials Science and Mechanical Engineering at Harvard University. Her focus is on self-assembly of inverse opals for optical and biomedical applications.

Joanna Aizenberg is Amy Smith Berylson Professor of Materials Science and Professor of Chemistry and Chemical Biology at Harvard University. She received her Ph.D. in Structural Biology from the Weizmann Institute of Science, following which she was a postdoctoral fellow at Harvard University and a member of the Bell Laboratories Technical Staff. Throughout her career, she has made a number of pioneering contributions in the field of bioinspired materials chemistry. Aizenberg is a member of the National Academy of Science, National Academy of Engineering, American Philosophical Society, and American Academy of Arts and Sciences.

ACKNOWLEDGMENTS

This Account is based upon work supported by the Harvard Materials Research Science and Engineering Center under the National Science Foundation Grant DMR-2011754 (synthesis and characterization), by the Department of Defense, Army Research Office under Award W911NF-17-1-0351 (optical applications), and as part of the Energy Frontier Research Center funded by the U.S. Department of Energy under Award DE-SC0012573 (applications in catalysis). N.J.N. is funded by the National Science Foundation Graduate Research Fellowship under Grant DGE1745303.

REFERENCES

(1) Hatton, B.; Mishchenko, L.; Davis, S.; Sandhage, K. H.; Aizenberg, J. Assembly of Large-Area, Highly Ordered, Crack-Free Inverse Opal Films. *Proc. Natl. Acad. Sci. U. S. A* **2010**, *107* (23), 10354−10359.

(2) Burgess, I. B.; Mishchenko, L.; Hatton, B. D.; Kolle, M.; Lončar, M.; Aizenberg, J. Encoding Complex Wettability Patterns in Chemically Functionalized 3D Photonic Crystals. *J. Am. Chem. Soc.* **2011**, *133* (32), 12430−12432.

(3) Li, L.; Goodrich, C.; Yang, H.; Phillips, K. R.; Jia, Z.; Chen, H.; Wang, L.; Zhong, J.; Liu, A.; Lu, J.; Shuai, J.; Brenner, M. P.; Spaepen, F.; Aizenberg, J. Microscopic Origins of the Crystallographically

Preferred Growth in Evaporation-Induced Colloidal Crystals. *Proc. Natl. Acad. Sci. U. S. A* **2021**, *118* (32), No. e2107588118.
(4) van der Hoeven, J. E. S.; Krämer, S.; Dussi, S.; Shirman, T.; Park, K. C. K.; Rycroft, C. H.; Bell, D. C.; Friend, C. M.; Aizenberg, J. On the Origin of Sinter-Resistance and Catalyst Accessibility in Raspberry-Colloid-Templated Catalyst Design. *Adv. Funct. Mater.* **2021**, *31* (49), 2106876.
(5) Phillips, K. R.; England, G. T.; Sunny, S.; Shirman, E.; Shirman, T.; Vogel, N.; Aizenberg, J. A Colloidoscope of Colloid-Based Porous Materials and Their Uses. *Chem. Soc. Rev.* **2016**, *45* (2), 281−322.
(6) Cai, Z.; Li, Z.; Ravaine, S.; He, M.; Song, Y.; Yin, Y.; Zheng, H.; Teng, J.; Zhang, A. From Colloidal Particles to Photonic Crystals: Advances in Self-Assembly and Their Emerging Applications. *Chem. Soc. Rev.* **2021**, *50* (10), 5898−5951.
(7) Stein, A.; Wilson, B. E.; Rudisill, S. G. Design and Functionality of Colloidal−Crystal−Templated Materials—Chemical Applications of Inverse Opals. *Chem. Soc. Rev.* **2013**, *42* (7), 2763−2803.
(8) Malitson, I. H. Interspecimen Comparison of the Refractive Index of Fused Silica. *J. Opt. Soc. Am.* **1965**, *55* (10), 1205.
(9) Devore, J. R. Present Time These Two Elements Do Not Occur Signifi- Cantly in Engine Deposits. *J. Opt. Soc. Am.* **1883**, 416−419.
(10) Chen, J. I. L.; Von Freymann, G.; Choi, S. Y.; Kitaev, V.; Ozin, G. A. Amplified Photochemistry with Slow Photons. *Adv. Mater.* **2006**, *18* (14), 1915−1919.
(11) Liu, J.; Zhao, H.; Wu, M.; Van der Schueren, B.; Li, Y.; Deparis, O.; Ye, J.; Ozin, G. A.; Hasan, T.; Su, B. L. Slow Photons for Photocatalysis and Photovoltaics. *Adv. Mater.* **2017**, *29* (17), 1605349.
(12) Han, J. H.; Shneidman, A. V.; Kim, D. Y.; Nicolas, N. J.; van der Hoeven, J. E. S.; Aizenberg, M.; Aizenberg, J. Highly Ordered Inverse Opal Structures Synthesized from Shape-Controlled Nanocrystal Building Blocks. *Angew. Chem., Int. Ed* **2022**, *61* (3), No. e202111048.
(13) Waterhouse, G. I. N.; Waterland, M. R. Opal and Inverse Opal Photonic Crystals: Fabrication and Characterization. *Polyhedron* **2007**, *26* (2), 356−368.
(14) Schroden, R. C.; Al-Daous, M.; Blanford, C. F.; Stein, A. Optical Properties of Inverse Opal Photonic Crystals. *Chem. Mater.* **2002**, *14* (8), 3305−3315.
(15) Phillips, K. R.; Shirman, T.; Shirman, E.; Shneidman, A. V.; Kay, T. M.; Aizenberg, J. Nanocrystalline Precursors for the Co-Assembly of Crack-Free Metal Oxide Inverse Opals. *Adv. Mater.* **2018**, *30* (19), 1706329.
(16) Phillips, K. R.; Vogel, N.; Hu, Y.; Kolle, M.; Perry, C. C.; Aizenberg, J. Tunable Anisotropy in Inverse Opals and Emerging Optical Properties. *Chem. Mater.* **2014**, *26* (4), 1622−1628.
(17) Phillips, K. R.; Vogel, N.; Burgess, I. B.; Perry, C. C.; Aizenberg, J. Directional Wetting in Anisotropic Inverse Opals. *Langmuir* **2014**, *30* (25), 7615−7620.
(18) Phillips, K. R.; Zhang, C. T.; Yang, T.; Kay, T.; Gao, C.; Brandt, S.; Liu, L.; Yang, H.; Li, Y.; Aizenberg, J.; Li, L. Fabrication of Photonic Microbricks via Crack Engineering of Colloidal Crystals. *Adv. Funct. Mater.* **2020**, *30* (26), 1908242.
(19) Shirman, E.; Shirman, T.; Shneidman, A. V.; Grinthal, A.; Phillips, K. R.; Whelan, H.; Bulger, E.; Abramovitch, M.; Patil, J.; Nevarez, R.; Aizenberg, J. Modular Design of Advanced Catalytic Materials Using Hybrid Organic−Inorganic Raspberry Particles. *Adv. Funct. Mater.* **2018**, *28* (27), 1704559.
(20) Luneau, M.; Shirman, T.; Filie, A.; Timoshenko, J.; Chen, W.; Trimpalis, A.; Flytzani-Stephanopoulos, M.; Kaxiras, E.; Frenkel, A. I.; Aizenberg, J.; Friend, C. M.; Madix, R. J. Dilute Pd/Au Alloy Nanoparticles Embedded in Colloid-Templated Porous SiO2: Stable Au-Based Oxidation Catalysts. *Chem. Mater.* **2019**, *31* (15), 5759−5768.
(21) Erola, M. O. A.; Philip, A.; Ahmed, T.; Suvanto, S.; Pakkanen, T. T. Fabrication of Au- and Ag-SiO2 Inverse Opals Having Both Localized Surface Plasmon Resonance and Bragg Diffraction. *J. Solid State Chem.* **2015**, *230*, 209−217.
(22) Gupta, G.; Patel, M. N.; Ferrer, D.; Heitsch, A. T.; Korgel, B. A.; Jose-Yacaman, M.; Johnston, K. P. Stable Ordered FePt Mesoporous Silica Catalysts with High Loadings. *Chem. Mater.* **2008**, *20* (15), 5005−5015.
(23) Vasquez, Y.; Kolle, M.; Mishchenko, L.; Hatton, B. D.; Aizenberg, J. Three-Phase Co-Assembly: In Situ Incorporation of Nanoparticles into Tunable, Highly Ordered, Porous Silica Films. *ACS Photonics* **2014**, *1* (1), 53−60.
(24) Shirman, T.; Toops, T. J.; Shirman, E.; Shneidman, A. V.; Liu, S.; Gurkin, K.; Alvarenga, J.; Lewandowski, M. P.; Aizenberg, M.; Aizenberg, J. Raspberry Colloid-Templated Approach for the Synthesis of Palladium-Based Oxidation Catalysts with Enhanced Hydrothermal Stability and Low-Temperature Activity. *Catal. Today* **2021**, *360*, 241−251.
(25) Vogel, N.; Utech, S.; England, G. T.; Shirman, T.; Phillips, K. R.; Koay, N.; Burgess, I. B.; Kolle, M.; Weitz, D. A.; Aizenberg, J. Color from Hierarchy: Diverse Optical Properties of Micron-Sized Spherical Colloidal Assemblies. *Proc. Natl. Acad. Sci. U. S. A* **2015**, *112* (35), 10845−10850.
(26) Wang, J.; Sultan, U.; Goerlitzer, E. S. A.; Mbah, C. F.; Engel, M.; Vogel, N. Structural Color of Colloidal Clusters as a Tool to Investigate Structure and Dynamics. *Adv. Funct. Mater.* **2020**, *30* (26), 1907730 DOI: 10.1002/adfm.201907730.
(27) Tan, A. T. L.; Beroz, J.; Kolle, M.; Hart, A. J. Direct-Write Freeform Colloidal Assembly. *Adv. Mater.* **2018**, *30* (44), 1803620.
(28) Schaffner, M.; England, G.; Kolle, M.; Aizenberg, J.; Vogel, N. Combining Bottom-Up Self-Assembly with Top-Down Microfabrication to Create Hierarchical Inverse Opals with High Structural Order. *Small* **2015**, *11* (34), 4334−4340.
(29) Kang, H.; Lee, J. S.; Chang, W. S.; Kim, S. H. Liquid-Impermeable Inverse Opals with Invariant Photonic Bandgap. *Adv. Mater.* **2015**, *27* (7), 1282−1287.
(30) Burgess, I. B.; Koay, N.; Raymond, K. P.; Kolle, M.; Lončar, M.; Aizenberg, J. Wetting in Color: Colorimetric Differentiation of Organic Liquids with High Selectivity. *ACS Nano* **2012**, *6* (2), 1427−1437.
(31) Nicolas, N. J.; Duffy, M. A.; Hansen, A.; Aizenberg, J. Inverse Opal Films for Medical Sensing: Application in Diagnosis of Neonatal Jaundice. *Adv. Healthc. Mater.* **2021**, *10* (4), 2001326 DOI: 10.1002/adhm.202001326.
(32) Yu, Y.; Brandt, S.; Nicolas, N. J.; Aizenberg, J. Colorimetric Ethanol Indicator Based on Instantaneous, Localized Wetting of a Photonic Crystal. *ACS Appl. Mater. Interfaces* **2020**, *12* (1), 1924−1929.
(33) Meng, L.; Wei, H.; Nagel, A.; Wiley, B. J.; Scriven, L. E.; Norris, D. J. The Role of Thickness Transitions in Convective Assembly. *Nano Lett.* **2006**, *6* (10), 2249−2253.
(34) Kaplan, C. N.; Wu, N.; Mandre, S.; Aizenberg, J.; Mahadevan, L. Dynamics of Evaporative Colloidal Patterning. *Phys. Fluids* **2015**, *27* (9), 092105.
(35) Phillips, K. R.; Shirman, T.; Aizenberg, M.; England, G. T.; Vogel, N.; Aizenberg, J. Silica-Titania Hybrids for Structurally Robust Inverse Opals with Controllable Refractive Index. *J. Mater. Chem. C* **2020**, *8* (1), 109−116.
(36) Tan, Y.; Qian, W.; Ding, S.; Wang, Y. Gold-Nanoparticle-Infiltrated Polystyrene Inverse Opals: A Three-Dimensional Platform for Generating Combined Optical Properties. *Chem. Mater.* **2006**, *18* (15), 3385−3389.
(37) Rothammer, M.; Zollfrank, C.; Busch, K.; von Freymann, G. Tailored Disorder in Photonics: Learning from Nature. *Adv. Opt. Mater.* **2021**, *9* (19), 2100787 DOI: 10.1002/adom.202100787.
(38) Mouchet, S. R.; Luke, S.; McDonald, L. T.; Vukusic, P. Optical Costs and Benefits of Disorder in Biological Photonic Crystals. *Faraday Discuss.* **2020**, *223*, 9−48.
(39) Yu, S.; Qiu, C. W.; Chong, Y.; Torquato, S.; Park, N. Engineered Disorder in Photonics. *Nat. Rev. Mater.* **2021**, *6* (3), 226−243.
(40) Koay, N.; Burgess, I. B.; Kay, T. M.; Nerger, B. A.; Miles-Rossouw, M.; Shirman, T.; Vu, T. L.; England, G.; Phillips, K. R.; Utech, S.; Vogel, N.; Kolle, M.; Aizenberg, J. Hierarchical Structural Control of Visual Properties in Self-Assembled Photonic-Plasmonic Pigments. *Opt. Express* **2014**, *22* (23), 27750.

(41) Joannopoulos, J. D.; Villeneuve, P. R.; Fan, S. Photonic Crystals Putting a New Twist on Light NATURE Joannopoulos 386143a0.Pdf. *Nature* **1997**, *386* (6621), 143−149.
(42) Baba, T. Slow Light in Photonic Crystals. *Nat. Photonics* **2008**, *2* (8), 465−473.
(43) Guldin, S.; Hüttner, S.; Kolle, M.; Welland, M. E.; Müller-Buschbaum, P.; Friend, R. H.; Steiner, U.; Tétreault, N. Dye-Sensitized Solar Cell Based on a Three-Dimensional Photonic Crystal. *Nano Lett.* **2010**, *10* (7), 2303−2309.
(44) Luneau, M.; Shirman, T.; Foucher, A. C.; Duanmu, K.; Verbart, D. M. A.; Sautet, P.; Stach, E. A.; Aizenberg, J.; Madix, R. J.; Friend, C. M. Achieving High Selectivity for Alkyne Hydrogenation at High Conversions with Compositionally Optimized PdAu Nanoparticle Catalysts in Raspberry Colloid-Templated SiO2. *ACS Catal.* **2020**, *10* (1), 441−450.
(45) Shahsafi, A.; Joe, G.; Brandt, S.; Shneidman, A. V.; Stanisic, N.; Xiao, Y.; Wambold, R.; Yu, Z.; Salman, J.; Aizenberg, J.; Kats, M. A. Wide-Angle Spectrally Selective Absorbers and Thermal Emitters Based on Inverse Opals. *ACS Photonics* **2019**, *6* (11), 2607−2611.
(46) Liu, J.; Liu, J.; Wu, P.; Zhang, M.; Wang, J.; Jiang, L. Multiple Solvent-Response Behavior of Metal-Organic Inverse Opals. *J. Photochem. Photobiol. A Chem.* **2018**, *355*, 125−130.
(47) Lee, W. S.; Kang, T.; Kim, S. H.; Jeong, J. An Antibody-Immobilized Silica Inverse Opal Nanostructure for Label-Free Optical Biosensors. *Sensors (Switzerland)* **2018**, *18* (1), 307.
(48) Singleton, T. A.; Burgess, I. B.; Nerger, B. A.; Goulet-Hanssens, A.; Koay, N.; Barrett, C. J.; Aizenberg, J. Photo-Tuning of Highly Selective Wetting in Inverse Opals. *Soft Matter* **2014**, *10* (9), 1325−1328.
(49) Xu, Q.; Mahpeykar, S. M.; Burgess, I. B.; Wang, X. Inverse Opal Photonic Crystals as an Optofluidic Platform for Fast Analysis of Hydrocarbon Mixtures. *ACS Appl. Mater. Interfaces* **2018**, *10* (23), 20120−20127.
(50) Vogel, N.; Belisle, R. A.; Hatton, B.; Wong, T. S.; Aizenberg, J. Transparency and Damage Tolerance of Patternable Omniphobic Lubricated Surfaces Based on Inverse Colloidal Monolayers. *Nat. Commun. 2013 41* **2013**, *4* (1), 1−10.
(51) Schellenberger, F.; Xie, J.; Encinas, N.; Hardy, A.; Klapper, M.; Papadopoulos, P.; Butt, H. J.; Vollmer, D. Direct Observation of Drops on Slippery Lubricant-Infused Surfaces. *Soft Matter* **2015**, *11* (38), 7617−7626.
(52) Wong, T. S.; Kang, S. H.; Tang, S. K. Y.; Smythe, E. J.; Hatton, B. D.; Grinthal, A.; Aizenberg, J. Bioinspired Self-Repairing Slippery Surfaces with Pressure-Stable Omniphobicity. *Nature* **2011**, *477* (7365), 443−447.
(53) Miao, S. S.; Wang, Y.; Zhao, Y. J.; Chen, Y. P. Bio-Inspired Slippery Surfaces with Multifunctional Anti-Icing Performance. *Sci. China Technol. Sci.* **2021**, *64* (10), 2110−2118.
(54) Liu, C.; Ding, H.; Wu, Z.; Gao, B.; Fu, F.; Shang, L.; Gu, Z.; Zhao, Y. Tunable Structural Color Surfaces with Visually Self-Reporting Wettability. *Adv. Funct. Mater.* **2016**, *26* (43), 7937−7942.
(55) Sun, L.; Wang, Y.; Zhang, X.; Bian, F.; Shang, L.; Zhao, Y.; Sun, W. Bio-Inspired Self-Replenishing and Self-Reporting Slippery Surfaces from Colloidal Co-Assembly Templates. *Chem. Eng. J.* **2021**, *426* (June), 131641.
(56) Adera, S.; Naworski, L.; Davitt, A.; Mandsberg, N. K.; Shneidman, A. V.; Alvarenga, J.; Aizenberg, J. Enhanced Condensation Heat Transfer Using Porous Silica Inverse Opal Coatings on Copper Tubes. *Sci. Rep* **2021**, *11* (1), 1−11.
(57) van der Hoeven, J. E. S.; Ngan, H. T.; Taylor, A.; Eagan, N. M.; Aizenberg, J.; Sautet, P.; Madix, R. J.; Friend, C. M. Entropic Control of HD Exchange Rates over Dilute Pd-in-Au Alloy Nanoparticle Catalysts. *ACS Catal.* **2021**, *11* (12), 6971−6981.
(58) Marcella, N.; Lim, J. S.; Płonka, A. M.; Yan, G.; Owen, C. J.; van der Hoeven, J. E. S.; Foucher, A. C.; Ngan, H. T.; Torrisi, S. B.; Marinkovic, N. S.; Stach, E. A.; Weaver, J. F.; Aizenberg, J.; Sautet, P.; Kozinsky, B.; Frenkel, A. I. Decoding Reactive Structures in Dilute Alloy Catalysts. *Nat. Commun.* **2022**, *13* (1), 1−9.
(59) Lee, J. D.; Miller, J. B.; Shneidman, A. V.; Sun, L.; Weaver, J. F.; Aizenberg, J.; Biener, J.; Boscoboinik, J. A.; Foucher, A. C.; Frenkel, A. I.; Van Der Hoeven, J. E. S.; Kozinsky, B.; Marcella, N.; Montemore, M. M.; Ngan, H. T.; O'Connor, C. R.; Owen, C. J.; Stacchiola, D. J.; Stach, E. A.; Madix, R. J.; Sautet, P.; Friend, C. M. Dilute Alloys Based on Au, Ag, or Cu for Efficient Catalysis: From Synthesis to Active Sites. *Chem. Rev.*, in press, DOI: 10.1021/acs.chemrev.1c00967.
(60) Wu, H.; Wang, D.; Schwartz, D. K. Connecting Hindered Transport in Porous Media across Length Scales: From Single-Pore to Macroscopic. *J. Phys. Chem. Lett.* **2020**, *11* (20), 8825−8831.
(61) Shirman, T.; Lattimer, J.; Luneau, M.; Shirman, E.; Reece, C.; Aizenberg, M.; Madix, R. J.; Aizenberg, J.; Friend, C. M. New Architectures for Designed Catalysts: Selective Oxidation Using AgAu Nanoparticles on Colloid-Templated Silica. *Chem. - A Eur. J.* **2018**, *24* (8), 1833−1837.

https://doi.org/10.1021/acs.accounts.2c00087
Acc. Chem. Res. 2022, 55, 1809−1820